

Electrically assisted light-induced gliding of nematic liquid-crystal easy axis at varying polarization azimuth of reorienting light: model and experiment

S.V. Pasechnik,^{1,2} A.V. Dubtsov,¹ D.V. Shmeliyova,¹ D.A. Semerenko,¹
V.G. Chigrinov,^{2,*} M.A. Sinenko,³ and Alexei D. Kiselev^{4,2,†}

¹*Moscow State University of Instrument Engineering and Computer Science,
Stromynka 20, 107846 Moscow, Russia*

²*Hong Kong University of Science and Technology,
Clear Water Bay, Kowloon, Hong Kong*

³*Chernigov State Technological University,
Shevchenko Street 95, 14027 Chernigov, Ukraine*

⁴*Institute of Physics of National Academy of Sciences of Ukraine,
prospekt Nauki 46, 03028 Kiev, Ukraine*

(Dated: November 5, 2018)

The phenomenological torque balance model previously introduced to describe the electrically assisted light-induced gliding is generalized to study the reorientation dynamics of the nematic liquid crystal easy axis at photoaligned azo-dye films under the combined action of in-plane electric field and reorienting UV light linearly polarized at varying polarization azimuth, φ_p . We systematically examine the general properties of the torque balance model by performing analysis of the bifurcations of equilibria at different values of the polarization azimuth and apply the model to interpret the experimental results. In our experiments, it is found that, in contrast to the case where $\varphi_p = 0$ and the light polarization vector is parallel to the initial easy axis, at $\varphi_p \neq 0$, the pronounced purely photoinduced reorientation is observed outside the interelectrode gaps. It is also observed that, in the regions between electrodes with non-zero electric field, the dynamics of reorientation slows down with φ_p and the sense of easy axis rotation is independent of the sign of φ_p .

PACS numbers: 61.30.Hn, 42.70.Gi

Keywords: nematic liquid crystal; easy axis gliding; photo-alignment; polarization azimuth

I. INTRODUCTION

It is well known that external electric, magnetic or light fields may produce deformations of liquid crystal (LC) orientational structures initially stabilized by anisotropic boundary surfaces (substrates). There is a variety of related Fréedericksz-type effects that are at the heart of operation of the vast majority of modern liquid crystal devices [1, 2].

Among the key factors that have a profound effect on behavior of the field induced orientational transitions are the boundary conditions at the substrates. These conditions are determined by the anchoring characteristics such as the anchoring energy strengths and

* Email address: eechigr@ust.hk

† Email address: kiselev@iop.kiev.ua

the *easy axis*, \mathbf{n}_e , giving the direction of preferential orientation of LC molecules at the surface.

In contrast to the traditional description of Fréedericksz-type transitions, it turned out that reorientation processes induced by external fields may additionally involve slow rotation of the easy axis. Over the past few decades this slow motion — the so-called *easy axis gliding* — has received much attention as a widespread phenomenon observed in a variety of liquid crystals on amorphous glass [3], polymer [4–13] and solid [6, 12] substrates.

Slow reorientation of the easy axis also takes place on the photosensitive layers prepared using the photoalignment (PA) technique. These include poly-(vinyl)-alcohol (PVA) coatings with embedded azo-dye molecules [5], polymer compound poly (vinyl methoxycinnamate) [7], and the azo-dye films [12].

The PA technique is employed in the manufacturing process of liquid crystal displays for fabricating high quality aligning substrates and uses linearly polarized ultraviolet (LPUV) light to induce anisotropy of the angular distribution of molecules in azo-dye containing photosensitive films [14]. In this method, the easy axis is determined by the polarization azimuth of the pumping LPUV light, whereas the azimuthal and polar anchoring strengths may depend on a number of the governing parameters such as the wavelength and the irradiation dose [15].

So, in a LC cell with the initially irradiated layer, subsequent illumination with reorienting light which polarization differs from the one used to prepare the layer can trigger the light-induced easy axis gliding. Such gliding may be of considerable interest for applications such as LC rewritable devices [16] and the effects of the *polarization azimuth*, φ_p , that characterizes orientation of the polarization vector of reorienting LPUV light, \mathbf{E}_{UV} will be of our primary concern.

More specifically, we consider how the polarization azimuth affects the reorientational dynamics of the electrically assisted light-induced azimuthal gliding of the easy axis that takes place on photoaligned azo-dye layers when irradiation of nematic LC (NLC) cells with LPUV light is combined with the application of ac in-plane electric field [17]. It was observed that, at certain combinations of the parameters such as the amplitude of electric field E , the light intensity, I_{UV} , the exposure time, t_{exp} , and the doze of the initial UV irradiation, D_p , the switching off relaxation considerably slows down up to few months. The switching on dynamics of the gliding for both the linearly polarized and the nonpolarized reorienting light was studied in [18]. In particular, the results of the papers [17, 18] demonstrate that the combined effect may be used as a tool to tune technical parameters of LC memory devices.

So, as compared to the case of purely light-induced reorientation of the easy axis governed by the effect of photoinduced ordering in azo-dye layers, the dynamics of the electrically assisted light-induced gliding can be additionally influenced by the electric field, E .

In previous studies [17, 18], the reorienting light was linearly polarized along the initial easy axis. In this paper, our goal is to study how the polarization azimuth influences the surface mediated reorientation processes that occur in NLC cells under the combined action of LPUV light and in-plane electric field.

The layout of the paper is as follows.

In Sec. II, we formulate our phenomenological torque balance model of electrically assisted photoinduced easy axis reorientation that takes into account the effects due to the polarization azimuth. Then, for the dynamical system representing the model, the regime of photosaturation is studied by analyzing the bifurcations of equilibria at different values of the polarization azimuth.

In Sec. III, after short description of the experimental procedure used to measure the azimuthal easy axis angle as a function of irradiation time, the theoretical curves computed from the model are compared with the experimental data measured at various values of the polarization azimuth.

Finally, in Sec. IV we discuss the results and make some concluding remarks.

II. TORQUE BALANCE MODEL

In this section, we carry out a theoretical investigation into the effects of the reorienting light polarization by using a generalized version of the phenomenological model formulated in Refs. [12, 17, 18] to describe the effect of electrically assisted light-induced azimuthal gliding. According to this model, the anchoring characteristics of the photoaligned layer such as the easy axis, \mathbf{n}_e , are determined by orientational order of LC molecules adsorbed by the azo-dye film.

Initially, after PA treatment made before the cell is filled with LC, ordering of the adsorbed molecules is dictated by the orientational order parameter of the azo dye layer induced by the initial irradiation with linearly polarized UV light, \mathbf{E}_0 . The initial direction of preferential orientation at the surface \mathbf{n}_0 is typically normal to the principal axis of the photoinduced anisotropy defined by the polarization vector \mathbf{E}_0 .

When the cell filled with LC is subsequently irradiated by the linearly polarized reorienting light \mathbf{E}_{UV} with the polarization azimuth which differs from the one used at the preparation stage for PA treatment of the azo-dye layer, adsorbed LC molecules undergo light-induced transitions. These transitions occur due to reorientation of azo-dye molecules interacting with the adsorbed LC layer. Thus this is the dynamics of photoinduced reordering of azo-dye molecules that underlies the effect of the reorienting light on the anchoring properties of the photoaligned layer [19].

The easy axis can also be influenced by applying an in-plane electric field \mathbf{E} in the direction perpendicular to \mathbf{n}_0 . This can be explained in terms of adsorption-desorption processes taking place in the near-surface layer.

Initially, in the absence of electric field, the surface director \mathbf{n}_s characterizing average orientation of LC molecules in the near-surface layer is directed along the easy axis \mathbf{n}_0 . So, the adsorption-desorption processes do not influence the undisturbed angular distributions of LC molecules in the adsorbed and near-surface layers which are initially identical.

An electric field \mathbf{E} produces a twist deformation on the distance ξ defined as the *electric coherence length*: $\xi = \frac{1}{E} \sqrt{K_t/(\varepsilon_0 \Delta\varepsilon)}$, where $\Delta\varepsilon$ is the electric permittivity anisotropy, K_t is the effective Frank elastic constant for the twist deformation. At $\Delta\varepsilon > 0$, under this electric-field-induced deformation, the surface director, \mathbf{n}_s , inclines towards the electric field $\mathbf{E} \perp \mathbf{n}_0$. The absorption-desorption processes involving exchange of molecules between the differently aligned (adsorbed and near-surface) layers will result in reorientation of adsorbed molecules. Note that, owing to low probability of adsorption-desorption events, noticeable changes may require very long periods of time.

In the phenomenological model [12, 17], orientation of the easy axis \mathbf{n}_e characterized by the azimuthal angle φ_e is defined by the balance of the two torques: the torque transmitted from the bulk by the near-surface layer and the viscous torque proportional to *the specific viscosity of gliding* γ_e . For the surface director \mathbf{n}_s with the azimuthal angle φ_s , the analogous balance involves the torque arising due to deviation of the surface director from the easy

axes (it is proportional to the surface anchoring energy strength W_s), the torque transmitted from the bulk and the viscous torque proportional to the *surface viscosity* γ_s .

The resulting system of balance torque equations for the easy axis and surface director azimuthal angles, φ_e and φ_s , reads

$$\gamma_e \frac{\partial \varphi_e}{\partial t} = K_E (\pi/2 - \varphi_s) - \frac{W_e}{2} \sin 2(\varphi_e - \varphi_m), \quad (1a)$$

$$\gamma_s \frac{\partial \varphi_s}{\partial t} = K_E (\pi/2 - \varphi_s) - \frac{W_s}{2} \sin 2(\varphi_e - \varphi_s), \quad (1b)$$

where K_E is the electric field induced torque coefficient inversely proportional to the electric coherence length ξ , W_e is the effective anchoring parameter which defines the strength of coupling between the easy axis \mathbf{n}_e and the initial state of surface orientation described by the vector \mathbf{n}_0 .

An important additional parameter is the phase shift φ_m that enters the second term on the right-hand side of Eq. (1a) and depends on the polarization azimuth of the reorienting light. In the field-free regime with $E = 0$ and $K_E = 0$, equation (1a) assumes the simplified form

$$\frac{\partial \varphi_e}{\partial t} = -\frac{W_e}{2\gamma_e} \sin 2(\varphi_e - \varphi_m), \quad (2)$$

giving the formula for the easy axis angle

$$\tan(\varphi_e(t) - \varphi_m) = \tan(\varphi_e(0) - \varphi_m) \exp[-t/t_e], \quad (3)$$

where $t_e = \gamma_e/W_e$ is the characteristic time of purely photoinduced easy axis reorientation, that represents the solution of Eq. (2). This formula describes the phase shift as the azimuthal angle characterizing the photosteady orientation of the easy axis: $\varphi_e^{(\text{st})} = \varphi_m$ ($\varphi_e^{(\text{st})} = \varphi_m + \pi/2$) at $W_e > 0$ ($W_e < 0$). Interestingly, in our recent paper [19], it was shown that, under certain assumptions, equation (2) can be derived from the diffusion model of photoinduced reordering in azo-dye films. In this case, it turned out that the phase shift φ_m equals the angle between the polarization vector of the reorienting light, \mathbf{E}_{UV} , and the axis directed along the normal to \mathbf{n}_0 .

Note that the two special cases where $\varphi_m = 0$ and $\varphi_m = \pi/2$ has been previously treated in Refs. [12, 17, 18]. In subsequent sections, the effects due to variations of the phase shift will be of our primary interest.

A. Bifurcation analysis of dynamical system

Before making comparison between the model and experiment, we shall dwell briefly on the general properties of the dynamical system (1) which can be conveniently recast into the following dimensionless form:

$$\frac{\partial \varphi_e}{\partial \tau} = \psi_s - w_e \sin 2(\varphi_e - \varphi_m) \equiv \Phi(\varphi_e, \psi_s), \quad \tau = t/\tau_e, \quad (4a)$$

$$\frac{\partial \psi_s}{\partial \tau} = \gamma \left\{ -\psi_s + w_s \sin 2(\varphi_e + \psi_s) \right\} \equiv \gamma \Psi(\varphi_e, \psi_s), \quad \psi_s \equiv \pi/2 - \varphi_s, \quad (4b)$$

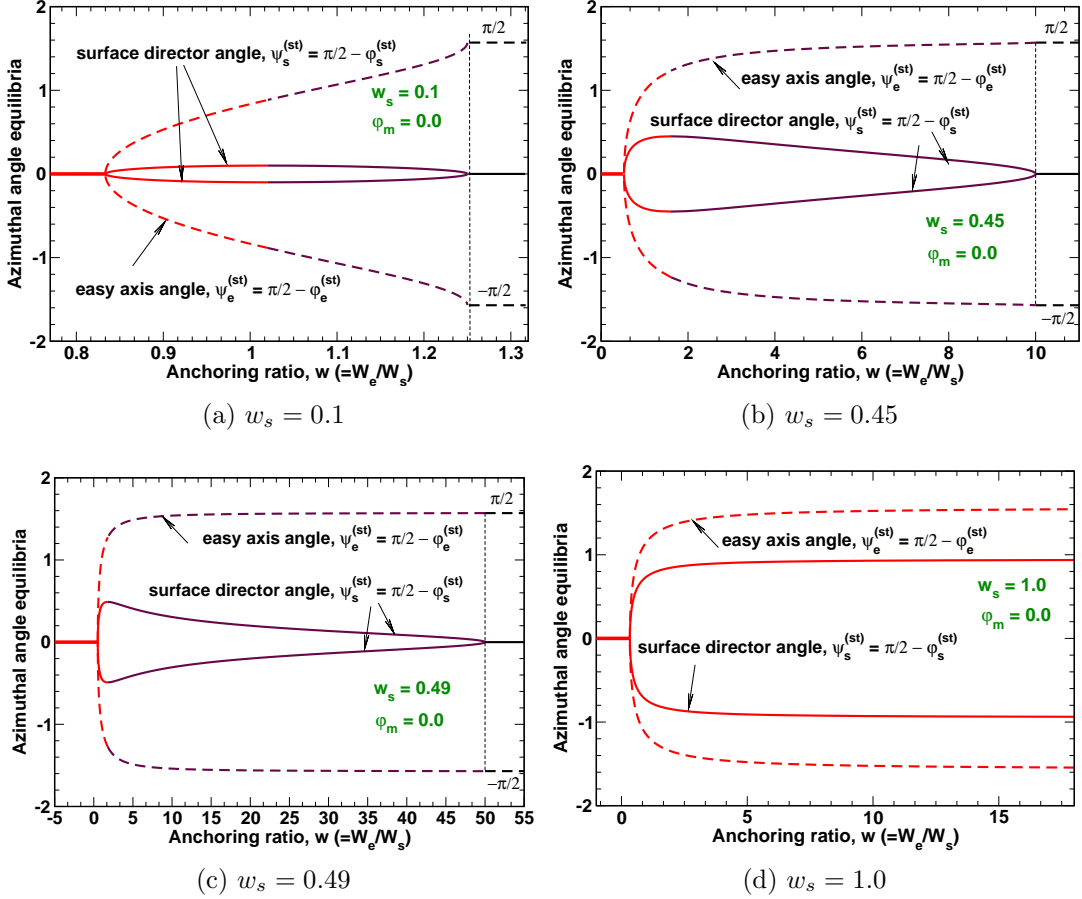


Figure 1: Bifurcation diagram for equilibria of easy axis and surface director azimuthal angles as a function of the anchoring ratio, $w = W_e/W_s$, at $\phi_m = 0$. Four cases are shown: (a) $w_s = 0.1$; (b) $w_s = 0.45$; (c) $w_s = 0.49$; and (d) $w_s = 1.0$.

where $\tau_e = \gamma_e/K_E$ is the characteristic time of easy axis reorientation; $\gamma = \gamma_e/\gamma_s$ is the viscosity ratio; $w_e = W_e/(2K_E)$ and $w_s = W_s/(2K_E)$ are the dimensionless anchoring parameters. The two symmetry relations

$$\varphi_m \rightarrow \varphi_m + \pi/2 \iff w_e \rightarrow -w_e, \quad (5a)$$

$$\varphi_m \rightarrow -\varphi_m \iff \{\varphi_e, \psi_s\} \rightarrow \{-\varphi_e, -\psi_s\} \quad (5b)$$

describe how the system (4) transforms when the phase shift is translated by $\pi/2$ (the polarization vector is rotated by $\pi/2$ around the z axis which is normal to the layer) and the phase shift changes its sign (the polarization vector is reflected with respect to the y axis).

The equilibrium (photosteady) states characterized by the azimuthal angles, $\varphi_e^{(st)} = \pi/2 - \psi_e^{(st)}$ and $\psi_s^{(st)} = \pi/2 - \varphi_s^{(st)}$, can be found as the stable (attracting) stationary points of the dynamical system (4). In this section we shall generalize the results of Ref. [18] where the equilibria have been studied in relation to the *anchoring ratio* $w = w_e/w_s = W_e/W_s$. In particular, our analysis enables us to relax the constraints requiring the anchoring parameter w_s to be small ($|w_s| < 0.5$) and the phase shift to be zero, $\varphi_m = 0$.

1. Branches of stationary states

Equations for the stationary solutions of the system (4) can be written in the following form:

$$\begin{cases} \sin 2(\varphi_e + \psi_s) = \psi_s/w_s, & \cos 2(\varphi_e + \psi_s) = -\frac{\mu}{w_s} \sqrt{w_s^2 - \psi_s^2}, \\ \sin 2(\varphi_e - \varphi_m) = \psi_s/w_e, & \cos 2(\varphi_e - \varphi_m) = \frac{\nu}{w_e} \sqrt{w_e^2 - \psi_s^2}, \end{cases} \quad (6)$$

where $\mu, \nu \in \{+1, -1\}$ are the indices numbering four different branches of the stationary states.

Similar to Ref. [18], our task is to examine behavior of the stationary solutions when the *anchoring ratio* $w = W_e/W_s$ varies whereas the anchoring parameter w_s and the phase shift φ_m are both kept constant. For this purpose, it is convenient to recast the stationarity equations (6) into the parametrized form

$$w = W_\nu(t; w_e) = t^{-1} \left\{ t \cos 2(t + \varphi_m) + \nu \sqrt{w_e^2 - t^2} \cos 2(t + \varphi_m) \right\}, \quad (7a)$$

$$w^{-1} = W_\mu^{(1)}(t; w_s) = t^{-1} \left\{ t \cos 2(t + \varphi_m) + \mu \sqrt{w_s^2 - t^2} \cos 2(t + \varphi_m) \right\}, \quad (7b)$$

where the surface director azimuthal angle ψ_s plays the role of a parameter $-|w_s| \leq t \equiv \psi_s \leq |w_s|$. Then the solutions of the equation

$$\frac{1}{W_\mu^{(1)}(t; w_s)} = W_\nu(t; w_s/W_\mu^{(1)}(t; w_s)) \Rightarrow t \in D_{\nu\mu} \quad (8)$$

form the branch of stationary points $D_{\nu\mu}$ and we can use Eq. (7b) to derive the relations

$$\psi_s^{(\text{st})}(w) = \begin{cases} w = \frac{1}{W_\mu^{(1)}(t; w_s)} \\ \psi_s^{(\text{st})} = t \end{cases}, \quad t \in D_{\nu\mu} \quad (9)$$

representing the dependence of the stationary values of the surface director angle on the anchoring ratio in the form of the parametrized curve in the $w - \psi_s$ plane. Similarly, in the $w - \psi_e$ plane, the curve

$$\psi_e^{(\text{st})}(w) = \begin{cases} w = \frac{1}{W_\mu^{(1)}(t; w_s)} \\ \psi_e^{(\text{st})} = t + 2^{-1} [\mu \arcsin(t/w_s) + (1 - \mu)\pi/2] \end{cases}, \quad t \in D_{\nu\mu}, \quad (10)$$

describes the corresponding branch of stationary easy axis angles.

We now pass on to the stability analysis of the stationary states. Following the standard approach [20, 21], the criteria of linearized stability are formulated in terms of the linearization matrix of the system (4), in the neighborhood of the fixed point $(\varphi_e^{(\text{st})}, \psi_s^{(\text{st})})$

$$\mathbf{H} = \begin{pmatrix} 1 & 0 \\ 0 & \gamma \end{pmatrix} \cdot \mathbf{\Lambda}, \quad \mathbf{\Lambda} = - \left(\begin{array}{cc} \frac{\partial \Phi}{\partial \varphi_e} & \frac{\partial \Phi}{\partial \psi_s} \\ \frac{\partial \Psi}{\partial \varphi_e} & \frac{\partial \Psi}{\partial \psi_s} \end{array} \right) \Big|_{\varphi_e = \varphi_e^{(\text{st})}, \psi_s = \psi_s^{(\text{st})}}, \quad (11)$$

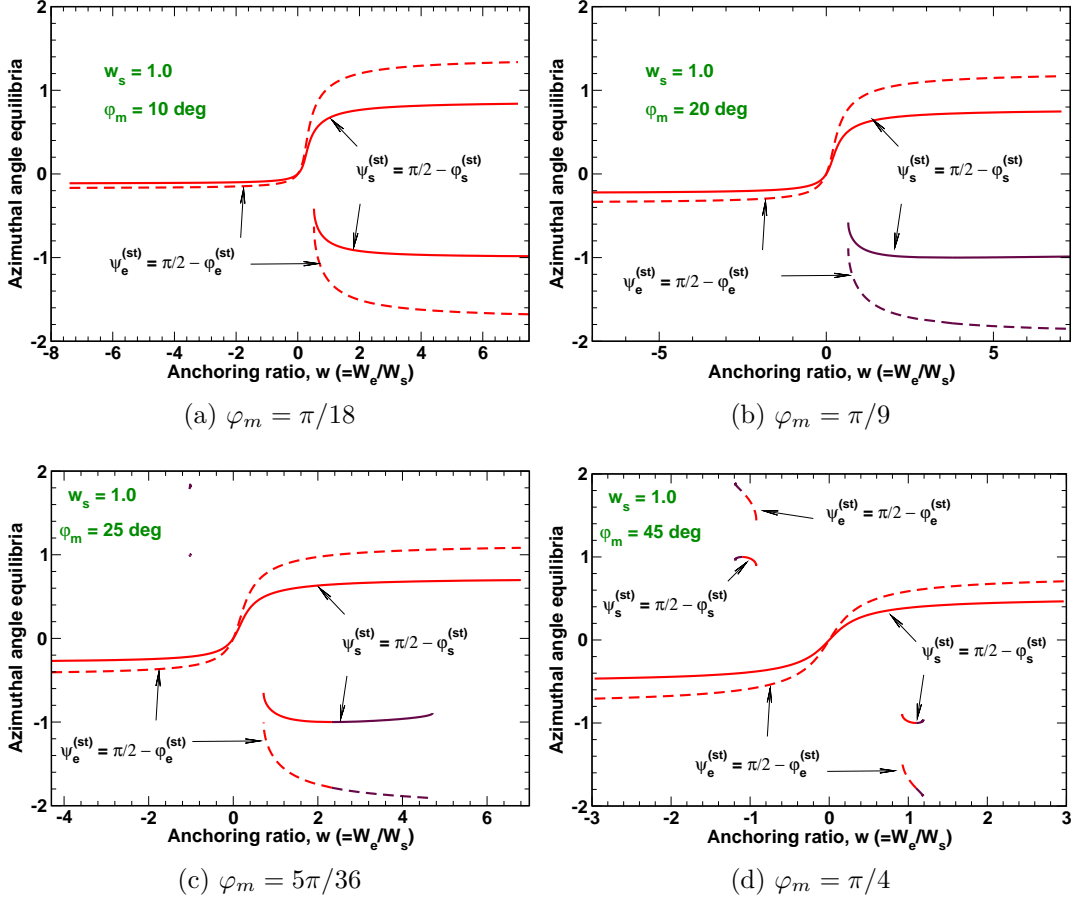


Figure 2: Bifurcation diagram for equilibria of easy axis and surface director azimuthal angles as a function of the anchoring ratio, $w = W_e/W_s$, at $w_s = 1.0$. Four cases are shown: (a) $\varphi_m = \pi/18$; (b) $\varphi_m = \pi/9$; (c) $\varphi_m = 5\pi/36$; and (d) $\varphi_m = \pi/4$.

so that, in the case of two-dimensional systems, the stability conditions are given by

$$\text{Tr } \mathbf{H} > 0, \quad \det \mathbf{H} > 0. \quad (12)$$

The expression for the matrix $\mathbf{\Lambda}$ evaluated for the branch of stationary points $D_{\nu\mu}$

$$\mathbf{\Lambda}|_{t \in D_{\nu\mu}} \equiv \mathbf{\Lambda}_{\nu\mu}(t) = \begin{pmatrix} 2\nu\sqrt{w_e^2 - t^2} & -1 \\ 2\mu\sqrt{w_s^2 - t^2} & 1 + 2\mu\sqrt{w_s^2 - t^2} \end{pmatrix} \quad (13)$$

can be derived with the help of equations (6).

2. Bifurcations of equilibria

The surface director equilibria are represented by the solutions of Eq. (8) that meet the stability conditions (12). These conditions combined with the formula (13) for the matrix $\mathbf{\Lambda}$ which enters the linearization matrix (11) can be analyzed using elementary methods to yield the following results: (a) D_{++} is the branch of stable stationary points (equilibria);

(b) the branch D_{--} is unstable; and (c) for the two remaining branches $D_{\nu\mu}$ with $\nu\mu = -1$, D_{-+} and D_{+-} , the stability conditions (12) are satisfied if and only if the determinant of the matrix $\mathbf{\Lambda}_{\nu\mu}$ is positive, $\det \mathbf{\Lambda}_{\nu\mu} > 0$. Thus the inequality

$$\nu\sqrt{[w_s/W_\mu^{(1)}(t; w_s)]^2 - t^2} \left(1 + 2\mu\sqrt{w_s^2 - t^2}\right) + \mu\sqrt{w_s^2 - t^2} > 0 \quad (14)$$

is the only stability condition that defines equilibria belonging to the branches D_{-+} and D_{+-} .

The bifurcation curves shown in Figs. 1 and 2 represent the surface director and easy axis equilibrium angles computed using the parametrizations given in Eqs. (9) and (10), respectively. The numerical procedure involves two steps: (a) solving equation (8) at $(\nu, \mu) \in \{(+, +), (+, -), (-, +)\}$; and (b) isolating the stable points of $D_{\nu\mu}$ with $\nu\mu = -1$ from the unstable ones based on the stability criterion (13).

Figure 1 demonstrate the effect of the anchoring parameter w_s on the bifurcation curves that describe dynamical behavior of the model (4) in relation the anchoring ratio $w = W_e/W_s$ when the phase shift is zero, $\varphi_m = 0$. The case of small anchoring parameter with $w_s < 1/2$ was studied in our previous paper [18] and is illustrated in Figs. 1a–1c.

It is seen that there is the only stationary value of the surface director angle, $\varphi_s^{(st)} = \pi/2$ ($\psi_s^{(st)} = 0$), provided that $w < w_+$ or $w > w_-$, where $w_\pm = 1/(1 \pm 2w_s)$ is the critical (bifurcation) value of the anchoring ratio. The equilibrium values of the easy axis angle in these two regions are: $\varphi_e^{(st)} = \pi/2$ ($\psi_e^{(st)} = 0$) at $w < w_+$ and $\varphi_e^{(st)} = 0$ ($\psi_e^{(st)} = \pi/2$) at $w > w_-$. The latter implies that, at large coupling parameter W_e when $w > w_-$, the easy axis gliding is completely suppressed, whereas, in the regime of weak coupling with $w < w_+$, the easy axis rotates approaching the stationary state of the surface director.

Referring to Figs. 1a–1c, when the anchoring ratio w passes through the critical points w_\pm the stationary state $\varphi_s^{(st)} = \pi/2$ becomes unstable and the pitchfork bifurcations [21] occur. So, for the surface director angle in the intermediate region with $w_+ < w < w_-$, there are two symmetrically arranged stable stationary points. In this case, gliding is not suppressed, but, by contrast to the regime of weak coupling, the equilibrium states of the easy axis and the surface director are no longer identical.

Now we examine the important case of large anchoring parameter w_s with $w_s > 1/2$ that represents the regime of weak electric field (low voltage). At $w_s = 1/2$, the largest critical value of the anchoring ratio w_- diverges and it can be expected that bifurcation diagrams at $w_s > 1/2$ are characterized by the only point of pitchfork bifurcation located at $w = w_+$. An example of such diagram is depicted in Fig. 1d.

In the zero-field limit with $E = 0$, the electric coherence length ξ and the parameter w_s both become infinitely large, whereas the bifurcation point w_+ decays to zero. From the formula (3), it is clear that the equilibrium angles at $w < w_+ = 0$ ($W_e < 0$) and $w > w_+ = 0$ ($W_e > 0$) are $\varphi_e^{(st)} = \varphi_s^{(st)} = \pi/2$ ($\psi_e^{(st)} = \psi_s^{(st)} = 0$) and $\varphi_e^{(st)} = \varphi_s^{(st)} = 0$ ($\psi_e^{(st)} = \psi_s^{(st)} = \pi/2$), respectively. So, reorientation of both the surface director and the easy axis is inhibited provided that the coupling constant W_e is positive.

Application of the electric field facilitates the process of reorientation. At non-vanishing voltage, the threshold value of the anchoring ratio is positive, $w_+ > 0$, and increases with electric field. As is shown in Fig. 1d, in the region of strong easy axis coupling where $w > w_+$, the angles $\psi_s^{(st)}$ and $\psi_e^{(st)}$ differ in magnitude, $|\psi_s^{(st)}| < |\psi_e^{(st)}|$. So, even at large values of the anchoring ratio w , reorientation of the surface director takes place as its magnitude is

below $\pi/2$. The latter is not the case for the easy axis because the magnitude of the easy axis angle $\psi_e^{(\text{st})}$ turned out to be very close to $\pi/2$.

From the symmetry relation (5b) it follows that, at $\varphi_m = 0$, bifurcation diagrams are invariant under reflection with respect to the w -axis: $(\psi_s^{(\text{st})}, \psi_e^{(\text{st})}) \rightarrow (-\psi_s^{(\text{st})}, -\psi_e^{(\text{st})})$ (see Fig. 1). Generally, this is no longer the case for nonzero phase shift.

Another important consequence of the symmetry relations (5) is that under the action of inversion in the origin of coordinates $(w, \psi_s^{(\text{st})}, \psi_e^{(\text{st})}) \rightarrow (-w, -\psi_s^{(\text{st})}, -\psi_e^{(\text{st})})$ the diagram computed at $\varphi_m = \pi/4 - \Delta\varphi_m$ transforms into the one with $\varphi_m = \pi/4 + \Delta\varphi_m$. Hence we can restrict ourselves to a set of the diagrams with the phase shift ranged between 0 and $\pi/4$, $\varphi_m \in [0, \pi/4]$.

The bifurcation curves presented in Fig. 2 illustrate the effect of the phase shift on the bifurcation diagrams at $w_s = 1$. As is evident from Fig. 2a, small variations of the phase shift play the role of a perturbation that splits the curves at the bifurcation point leading to the formation of the pattern consisting of two separated branches of equilibria. Such pattern is characteristic of perturbed (imperfect) pitchfork bifurcations [22, 23].

From Figs. 2b–2d, it can be seen that, when the phase shift increases, the low-lying branch of equilibria shrinks and, in the upper half of the diagram, additional branch develops. This branch grows with the phase shift up to the endpoint $\varphi_m = \pi/4$ of the interval $[0, \pi/4]$. As is illustrated in Fig. 2d, at this point, the bifurcation diagram is center symmetric and the bifurcation curves remain intact under the action of inversion: $(w, \psi_s^{(\text{st})}, \psi_e^{(\text{st})}) \rightarrow (-w, -\psi_s^{(\text{st})}, -\psi_e^{(\text{st})})$.

III. EXPERIMENT

In our experiments, liquid crystal (LC) cells ($d = 17.4 \pm 0.2 \mu\text{m}$) of sandwich like type were assembled between two amorphous glass plates. The upper glass plate was covered with a rubbed polyimide film to yield the strong planar anchoring conditions. In Fig. 3, the direction of rubbing gives the easy axis parallel to the x axis.

A film of the azobenzene sulfonic dye SD1 (Dainippon Ink and Chemicals) [14] was deposited onto the bottom substrate on which transparent indium tin oxide (ITO) electrodes were placed. The electrodes and the interelectrode stripes (the gap was about $g = 50 \mu\text{m}$) were arranged to be parallel to the x axis [see Fig. 3(a)].

As in [17, 18], the azo-dye SD1 layer was initially illuminated by linearly polarized UV light (LPUV) at the wavelength $\lambda = 365 \text{ nm}$. The preliminary irradiation produced the zones of different energy dose exposure $D_p = 0.27, 0.55 \text{ J/cm}^2$ characterized by relatively weak azimuthal anchoring strength. The light propagating along the normal to the substrates (the z axis) was selected by an interference filter. Orientation of the polarization vector of UV light, \mathbf{E}_0 , was chosen so as to align azo-dye molecules at a small angle of 4 degrees to the x axis, $\varphi_0 \approx 4 \text{ deg}$ [see Fig. 3(c)].

The LC cell was filled with the nematic LC mixture E7 (Merck) in isotropic phase and then slowly cooled down to room temperature. Thus we prepared the LC cell with a weakly twisted planar orientational structure where the director at the bottom surface \mathbf{n}_0 is clockwise rotated through the initial twist angle $\varphi_0 \approx 4 \text{ deg}$ which is the angle between \mathbf{n}_0 and the director at the upper substrate (the x axis).

As is indicated in figure 3(b), the director field deforms when the in-plane ac voltage ($U = 100 \text{ V}$, $f = 3 \text{ kHz}$) is applied to the electrodes. In addition to the electric field, $E =$

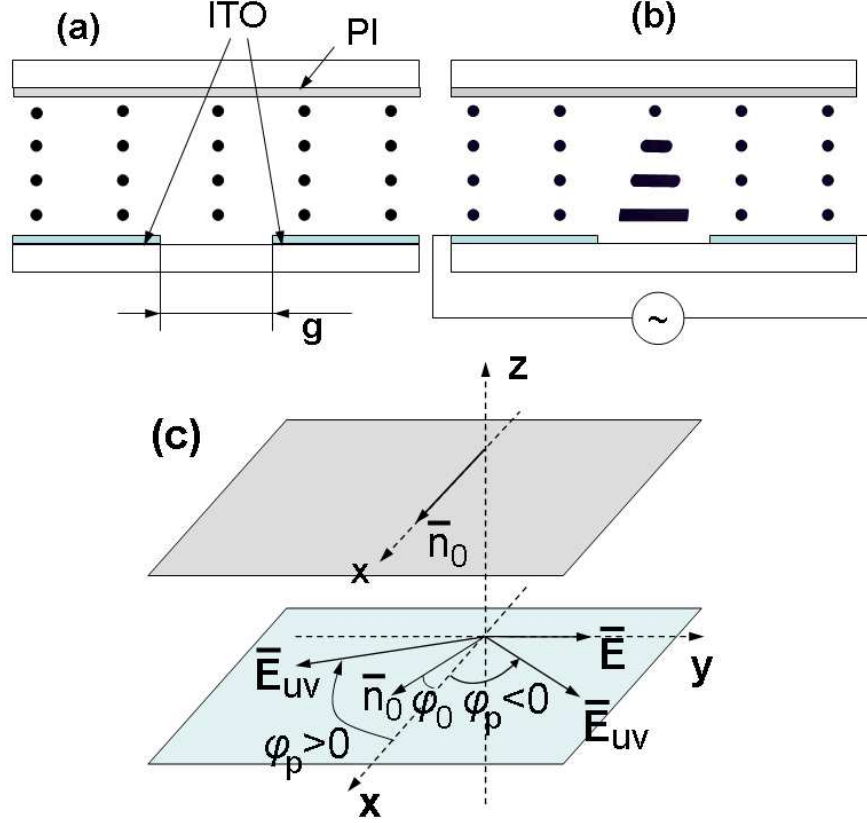


Figure 3: Geometry of the experiment: (a) initial state with $\mathbf{n}_0 = \hat{\mathbf{x}}$; (b) switching on an in-plane electric field, $\mathbf{E} = E\hat{\mathbf{x}}$, combined with LPUV irradiation; (c) the system of reference: the polarization vector \mathbf{E}_{UV} of the LPUV light wave propagating along the normal to the substrate (the z axis) is characterized by the polarization azimuth φ_p .

$2 \text{ V}/\mu\text{m}$, the cell was irradiated with the reorienting LPUV light beam ($I_{UV} = 0.26 \text{ mW}/\text{cm}^2$ and $\lambda = 365 \text{ nm}$) normally impinging onto the bottom substrate.

For this secondary LPUV irradiation, orientation of the polarization plane is determined by the *polarization azimuth*, φ_p , which is defined as the angle between the polarization vector of UV light, \mathbf{E}_{UV} , and the x axis. As is indicated in Fig. 3(c), we shall assume that positive (negative) values of the polarization azimuth, $\varphi_p > 0$ ($\varphi_p < 0$), correspond to clockwise (counterclockwise) rotation of the polarizer from the x axis to \mathbf{E}_{UV} .

Our experimental method has already been described in [17, 18, 24]. In this method, NLC orientational structures were observed via a polarized microscope connected with a digital camera and a fiber optics spectrometer. The rotating polarizer technique was used to measure the azimuthal angle φ_e characterizing orientation of the easy axis. In order to register microscopic images and to measure the value of φ_e , the electric field and the reorienting light were switched off for about 1 min. This time interval is short enough to ensure that orientation of the easy axis remains essentially intact in the course of measurements. The measurements were carried out at a temperature of 26°C .

When the electric field ($E = 2 \text{ V}/\mu\text{m}$) in combination with reorienting LPUV light of the intensity $I_{UV} = 0.26 \text{ mW}/\text{cm}^2$ is applied for more than 120 minutes, we observed the memory effect. In this case, after switching off the field and light, the easy axis did not relax

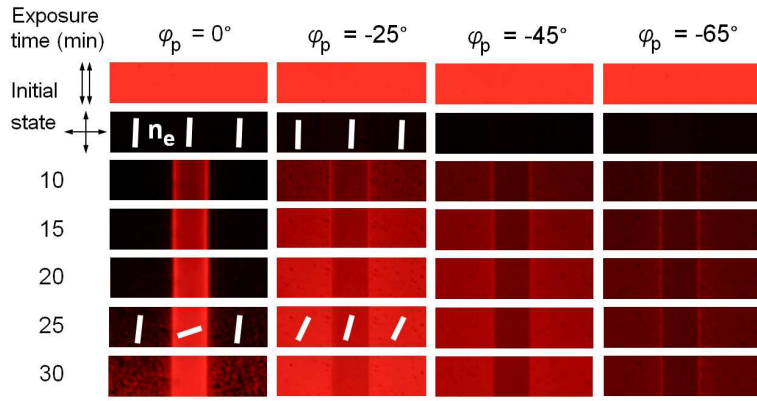


Figure 4: Microscopic images of the cell (filter with $\lambda = 630$ nm was used) in crossed polarizers for LPUV irradiation at different exposure times for various values of the polarization azimuth. The interelectrode gap ($g = 50 \mu\text{m}$) is indicated. The ac electric field is $E = 2 \text{ V}/\mu\text{m}$ and the initial irradiation dose is $D_p = 0.27 \text{ J}/\text{cm}^2$.

back to its initial state for at least few months.

A. Results

Figure 4 shows the microscopic images obtained at various times of irradiation by reorienting LPUV light for four different values of the polarization azimuth: $\varphi_p = 0, -24, -45, -65$ degrees. In this case, the initial irradiation dose is fixed at $D_p = 0.27 \text{ J}/\text{cm}^2$.

It can be seen that, when the reorienting light is linearly polarized along the initial surface director \mathbf{n}_0 and $\varphi_p = 0$, the brightness of stripes within the interelectrode gaps is much higher as compared to the ones in the region outside the gaps where the electric field is negligibly small $E \approx 0 \text{ V}/\mu\text{m}$. So, in the case of vanishing polarization azimuth studied in Refs. [17, 18], we arrive at the conclusion that, by contrast to the electrically assisted light-induced gliding, the purely photoinduced reorientation is almost entirely inhibited.

The latter is no longer the case for the reorienting light with nonzero polarization azimuth. Referring to Fig. 4, at $\varphi_p \neq 0$, light-induced distortions of the surface director in the zero-field region located outside the gaps are very much more pronounced. It is also evident from the curves depicted in Fig. 5(a) representing the irradiation time dependencies of the easy axis angle measured at negative polarization azimuthal angles of the reorienting LPUV light.

In the zero-field curves, the easy axis angle increases with the irradiation time starting from the angle of initial twist, φ_0 , and approaches the photo-steady state characterized by the photosaturated value of the angle close to $\pi/2 + \varphi_p$. The curves describing the electrically assisted reorientation within the interelectrode gaps lie below the zero-field ones and reveal analogous behavior.

The data measured at the initial irradiation dose $D_p = 0.55 \text{ J}/\text{cm}^2$. for the polarization azimuths of the opposite sign, $\varphi_p > 0$, (see Fig. 5(b)-(d)) show that, in the zero-field region, the light-induced changes of the easy axis angle are negative and correspond to the counterclockwise rotation of the polarizer. As seen from Fig. 5(b)-(d), the dynamics of the easy axis in the presence of the electric field essentially differs from the one in the regime of

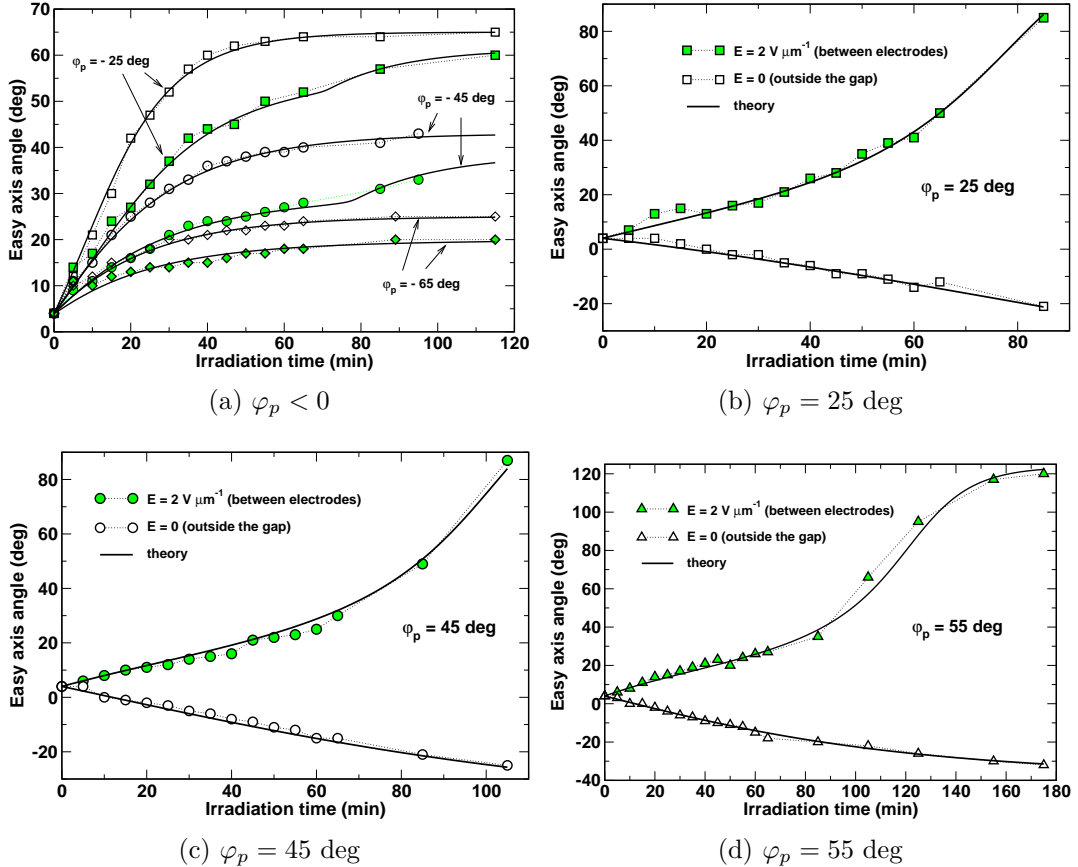


Figure 5: Easy axis angle as a function of the irradiation time measured for the reorienting LPUV light with different values of the polarization azimuth φ_p : (a) $\varphi_p < 0$ ($D_p = 0.27 \text{ J}/\text{cm}^2$) and (b)-(d) $\varphi_p > 0$ ($D_p = 0.55 \text{ J}/\text{cm}^2$). Open (solid) circles, squares and diamonds represent the data measured in the regions within (outside) the interelectrode gaps where $E = 2 \text{ V}/\mu\text{m}$ ($E \approx 0 \text{ V}/\mu\text{m}$). The results computed from the phenomenological model by solving equations (1a) and (1b) are shown as solid lines.

purely photoinduced reorientation.

In the interelectrode gaps, it turned out that the electric field prevails thus suppressing the tendency for the easy axis to be reoriented along the normal to the polarization vector of light \mathbf{E}_{UV} . This effect is illustrated in figure 6 that, in particular, presents the microscopic images registered in the dark states of both the zero-field and the interelectrode regions. It is indicated that the azimuthal angles describing orientation of the polarizer (and of the easy axis) in these states are opposite in sign.

B. Model versus experiment

Now we briefly discuss how the experimental data can be interpreted using the above phenomenological model. According to this model, the dynamics of the easy axis and surface director azimuthal angles, φ_e and φ_s , is governed by the system of balance torque equations (1).

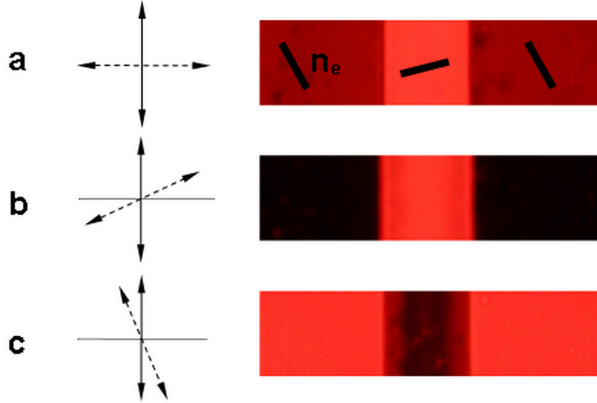


Figure 6: Microscopic images obtained at $\varphi_p > 0$ for different orientations of the polarizer: (a) crossed polarizers; dark state orientation for the regions (b) outside and (c) within the interelectrode gaps.

We can apply the formula (3) to fit the experimental data measured outside the interelectrode gaps. For $\varphi_p < 0$ and $D_p = 0.27 \text{ J/cm}^2$, the theoretical curves presented in figure 5(a) are computed at $t_e \approx 23 \text{ min}$. The values of φ_m are: $\varphi_m = 25 \text{ deg}$ at $\varphi_p = -65 \text{ deg}$; $\varphi_m = 43 \text{ deg}$ at $\varphi_p = -45 \text{ deg}$; and $\varphi_m = 65 \text{ deg}$ at $\varphi_p = -25 \text{ deg}$. Similarly, for the case where $\varphi_p > 0$ and $D_p = 0.55 \text{ J/cm}^2$, the results shown in figure 5(b) are computed at $t_e \approx 85 \text{ min}$. In this case, the values of φ_m are: $\varphi_m = -38 \text{ deg}$ at $\varphi_p = 55 \text{ deg}$; $\varphi_m = -43 \text{ deg}$ at $\varphi_p = 45 \text{ deg}$; and $\varphi_m = -65 \text{ deg}$ at $\varphi_p = 25 \text{ deg}$.

In the presence of electric field (the region between the electrodes), the dynamical system (1) has to be solved numerically. As in the previous section, it is convenient to work with the system rewritten in the dimensionless form (4) which is characterized by the characteristic time $\tau_e = \gamma_e/K_e$, the viscosity ratio $\gamma = \gamma_e/\gamma_s$ and the two dimensionless anchoring parameters: $w_e = W_e/(2K_E)$ and $w_s = W_s/(2K_E)$.

The parameters used for computing the curves shown in figure 5(a) ($\varphi_p < 0$ and $D_p = 0.27 \text{ J/cm}^2$): $\tau_e = 230 \text{ min}$, $\gamma = 100$ (the gliding viscosity is typically several orders higher than the surface viscosity), $w_e = 5$ and $w_s = 1$. The values of φ_m are: $\varphi_m = 25.1 \text{ deg}$ at $\varphi_p = -65 \text{ deg}$; $\varphi_m = 35 \text{ deg}$ at $\varphi_p = -45 \text{ deg}$; and $\varphi_m = 60 \text{ deg}$ at $\varphi_p = -25 \text{ deg}$. In figure 5(b) representing the case where $\varphi_p > 0$ and $D_p = 0.55 \text{ J/cm}^2$, the theoretical results are calculated at $\tau_e \approx 39.2 \text{ min}$, $\gamma = 100$, $w_e = 1.1$, $w_s = 10$ and the values of φ_m listed as follows: $\varphi_m = -41 \text{ deg}$ at $\varphi_p = 55 \text{ deg}$; $\varphi_m = -45 \text{ deg}$ at $\varphi_p = 45 \text{ deg}$; and $\varphi_m = -50 \text{ deg}$ at $\varphi_p = 25 \text{ deg}$.

As it can be seen from figures 5(a)-(b), the computed curves are in good agreement with the experimental data. The results of fitting indicate that the initial irradiation dose has a profound effect on the anchoring parameters, whereas the electric field affects the polarization dependent phase shift φ_m .

IV. DISCUSSION AND CONCLUSIONS

In conclusion, we have experimentally studied the effects of polarization azimuth in the electrically assisted light-induced azimuthal gliding of the NLC easy axis on the photoaligning azo-dye film. It is found that, by contrast to the case where the polarization vector

is oriented along the initial surface director, at nonzero polarization angle φ_0 , the purely photoinduced reorientation takes place outside the interelectrode gaps. For such field-free regime of reorientation, the easy axis reorients approaching the photosaturation limit close to the normal to the polarization vector. These results agree with the theoretical predictions of the diffusion model [25] describing kinetics of photoinduced ordering in azo-dye films and the corresponding theoretical analysis will be published in a separate paper.

In the regions between electrodes with non-vanishing electric field, the dynamics of reorientation slows down with the polarization azimuth and, as opposed to the case of purely photoinduced reorientation, the sense of easy axis rotation for the electrically assisted light-induced gliding is found to be independent of the sign of polarization azimuth. The above mentioned theory [25] cannot be directly applied to this case and we have shown that the phenomenological model [12, 17] can be extended to interpret our data.

ACKNOWLEDGMENTS

This work was partially supported by grants: RF Ministry of Education and Science: 14.B37.21.0894, 14.B37.21.1198, 14.B37.21.1914; CERG Grant 612310 and 612409.

-
- [1] D.-K. Yang and S.-T. Wu, *Fundamentals of Liquid Crystal Devices*, Series in Display Technology (Wiley, Chichester, 2006) p. 378.
 - [2] V. G. Chigrinov, *Liquid crystal devices: Physics and Applications* (Artech House, Boston, 1999) p. 357.
 - [3] E. A. Oliveira, A. M. Figueiredo Neto, and G. Durand, “Gliding anchoring of lyotropic nematic liquid crystals on amorphous glass surfaces,” *Phys. Rev. A* **4**, R825–R827 (1991).
 - [4] P. Vetter, Y. Ochmura, and T. Uchida, “Study of memory alignment of nematic liquid crystals on polyvinyl alcohol coatings,” *Jpn. J. Appl. Phys.* **32**, L1239–L1241 (1993).
 - [5] V. P. Vorflusev, H-S Kitzerow, and V. Chigrinov, “Azimuthal surface gliding of a nematic liquid crystal,” *Appl. Phys. Lett.* **70**, 3359 (1997).
 - [6] S. Faetti, M. Nobili, and I. Raggi, “Surface reorientation dynamics of nematic liquid crystals,” *Eur. Phys. J. B* **11**, 445–453 (1999).
 - [7] V. V. Lazarev, R. Barberi, M. Iovane, L. Papalino, and L. M. Blinov, “Dynamics of liquid crystal azimuthal anchoring at a poly (vinyl cinnamate) interface *in situ* during polarized UV light irradiation,” *Liq. Cryst.* **29**, 273–279 (2002).
 - [8] I. Jánossy and T. I. Kósa, “Gliding of liquid crystals on soft polymer surfaces,” *Phys. Rev. E* **70**, 052701 (2004).
 - [9] S. Joly, K. Antonova, P. Martinot-Lagarde, and I. Dozov, “Zenithal gliding of the easy axis of nematic liquid crystal,” *Phys. Rev. E* **70**, 050701(R) (2004).
 - [10] S. Faetti and P. Marianelli, “Strong azimuthal anchoring energy at a nematic-polyimide interface,” *Phys. Rev. E* **72**, 051708 (2005).
 - [11] S. Faetti and P. Marianelli, “Azimuthal director gliding at a strongly anchoring interface of polyimide,” *Liq. Cryst.* **33**, 327–334 (2006).
 - [12] S. V. Pasechnik, V. G. Chigrinov, D. V. Shmeliova, V. A. Tsvetkov, V. N. Kremenetsky, L. Zhijian, and A. V. Dubtsov, “Slow relaxation processes in nematic liquid crystals at weak surface anchoring,” *Liq. Cryst.* **33**, 175–185 (2006).

- [13] I. Jánossy, “Kinetics of director gliding on a polymer-liquid-crystal interface,” *Phys. Rev. E* **81**, 031714 (2010).
- [14] V. G. Chigrinov, V. M. Kozenkov, and H.-S. Kwok, *Photoalignment of Liquid Crystalline Materials: Physics and Applications*, Series in Display Technology (Wiley, Chichester, 2008) p. 219.
- [15] A. D. Kiselev, V. G. Chigrinov, and D. D. Huang, “Photo-induced ordering and anchoring properties of azo-dye films,” *Phys. Rev. E* **72**, 061703 (2005).
- [16] A. Muravsky, A. Murauski, V. Chigrinov, and H.-S. Kwok, “Light printing of grayscale pixel images on optical rewritable electronic paper,” *Jpn. J. Appl. Phys.* **47**, 6347–6353 (2008).
- [17] S. V. Pasechnik, A. V. Dubtsov, D. V. Shmeliova, V. A. Tsvetkov, and V. G. Chigrinov, “Effect of combined action of electric field and light on gliding of the easy axis in nematic liquid crystals,” *Liq. Cryst.* **35**, 569–579 (2008).
- [18] A. V. Dubtsov, S. V. Pasechnik, Alexei D. Kiselev, D. V. Shmeliova, and V. G. Chigrinov, “Electrically assisted light-induced azimuthal gliding of the nematic liquid-crystal easy axis on photoaligned substrates,” *Phys. Rev. E* **82**, 011702 (2010).
- [19] Alexei D. Kiselev, V. G. Chigrinov, S. V. Pasechnik, and A. V. Dubtsov, “Photoinduced reordering in thin azo-dye films and light-induced reorientation dynamics of the nematic liquid-crystal easy axis,” *Phys. Rev. E* **86**, 011706 (2012).
- [20] Yu. A. Kuznetsov, *Elements of Applied Bifurcation Theory*, 2nd ed., Applied Mathematical Sciences, Vol. 112 (Springer, NY, 1998) p. 592.
- [21] John Guckenheimer and Philip Holmes, *Nonlinear oscillations, dynamical systems, and bifurcations of vector fields*, Applied Mathematical Sciences, Vol. 42 (Springer-Verlag, NY, 1990) p. 459.
- [22] G. Iooss and D. D. Joseph, *Elementary Stability and Bifurcation Theory*, 2nd ed., Undergraduate Texts in Mathematics (Springer-Verlag, NY, 1990) p. 324.
- [23] J. D. Crawford, “Introduction to bifurcation theory,” *Rev. Mod. Phys.* **63**, 991–1037 (1991).
- [24] A. V. Dubtsov, D. V. Shmeliova, S. V. Pasechnik, Alexei D. Kiselev, and V. G. Chigrinov, “Effects of polarization azimuth in dynamics of electrically assisted light-induced gliding of nematic liquid-crystal easy axis,” *Appl. Phys. Lett.* **100**, 141608 (2012).
- [25] A. D. Kiselev, V. G. Chigrinov, and H.-S. Kwok, “Kinetics of photoinduced ordering in azo-dye films: Two-state and diffusion models,” *Phys. Rev. E* **80**, 011706 (2009).